Individual error correction drives responsive self-assembly of army ant scaffolds

Matthew J. Lutz[a,b,c,1,2], Chris R. Reid[d,1,2], Christopher J. Lustri[e], Albert B. Kao[f], Simon Garnier[g], and Iain D. Couzin[a,b,c]

[a]Department of Collective Behaviour, Max Planck Institute of Animal Behavior, Konstanz D-78457, Germany; [b]Centre for the Advanced Study of Collective Behaviour, University of Konstanz, Konstanz D-78457, Germany; [c]Department of Biology, University of Konstanz, Konstanz D-78457, Germany; [d]Department of Biological Sciences, Macquarie University, Sydney, NSW 2109, Australia; [e]Department of Mathematics and Statistics, Macquarie University, Sydney, NSW 2109, Australia; [f]Santa Fe Institute, Santa Fe, NM 87501; and [g]Department of Biological Sciences, New Jersey Institute of Technology, Newark, NJ 07102

Edited by Raghavendra Gadagkar, Indian Institute of Science, Bangalore, India, and approved March 5, 2021 (received for review July 9, 2020)

An inherent strength of evolved collective systems is their ability to rapidly adapt to dynamic environmental conditions, offering resilience in the face of disruption. This is thought to arise when individual sensory inputs are filtered through local interactions, producing an adaptive response at the group level. To understand how simple rules encoded at the individual level can lead to the emergence of robust group-level (or distributed) control, we examined structures we call "scaffolds," self-assembled by *Eciton burchellii* army ants on inclined surfaces that aid travel during foraging and migration. We conducted field experiments with wild *E. burchellii* colonies, manipulating the slope over which ants traversed, to examine the formation of scaffolds and their effects on foraging traffic. Our results show that scaffolds regularly form on inclined surfaces and that they reduce losses of foragers and prey, by reducing slipping and/or falling of ants, thus facilitating traffic flow. We describe the relative effects of environmental geometry and traffic on their growth and present a theoretical model to examine how the individual behaviors underlying scaffold formation drive group-level effects. Our model describes scaffold growth as a control response at the collective level that can emerge from individual error correction, requiring no complex communication among ants. We show that this model captures the dynamics observed in our experiments and is able to predict the growth—and final size—of scaffolds, and we show how the analytical solution allows for estimation of these dynamics.

self-assembly | resilience | collective behavior | distributed control | infrastructure

Complex infrastructures of all kinds, whether technological, social, or biological, demand one thing above all else to function effectively: the property of resilience in the face of disruption. In this context, we consider a resilient system to be one "that returns to or exceeds its predisturbance level of performance following a perturbation," as defined by Middleton and Latty in ref. 1. Understanding how resilience can be achieved in systems with many interacting components has emerged as a common goal across the disciplines of biology, engineering, and ecology (1, 2), and thus, it is important to identify and examine specific cases of infrastructural resilience in nature. Such examples abound among the social insects, in which difficult coordination problems are often solved through distributed control mechanisms relying on individual sensing and local interactions mediated by simple rules, without the need for complex communication (3, 4). Just as human societies rely on the organized flow of materials and information to function effectively, from the scale of the city to global trade networks (5–8), for many social insects, colony survival often depends on the effective coordination of foraging traffic to transport resources through the environment (9–11). These networks must be able to maintain their functionality when confronted with disruption and self-heal or otherwise rapidly respond to unpredictable conditions.

To achieve resilience, biological systems at many scales, including these social insect infrastructures, utilize various mechanisms of feedback control. In a recent example, a core regulatory feedback mechanism common to many social insects was identified—the so-called common stomach—which achieves resilience through a saturation process that relies on negative feedback through integral control (12). Both positive and negative feedback have long been known to underlie self-organizing processes like the formation of ant foraging trails and collective decision making (13–15), and negative feedback has been shown to play a particularly important role among social insects in maintaining flexibility when environmental conditions change (16–18). Understanding how feedback control operates in distributed systems, like ant colonies, to facilitate resilience remains an important challenge, with implications across disciplines.

The army ant *Eciton burchellii*, with large colonies of more than 500,000 workers and a distinctive nomadic life cycle (19), presents an ideal model for studying resilience and distributed control in natural systems. *E. burchellii* is considered a top predator in the neotropical forest leaf litter community (20) and a canonical example of self-organization among social insects (21).

Significance

Human-designed infrastructures and networks relying on centralized or hierarchical control are susceptible to single-point catastrophic failure when disrupted. By contrast, most complex biological systems employ distributed control and can be more robust to perturbations. In field experiments with *Eciton burchellii* army ants, we show that scaffold structures, self-assembled by living ants, emerge in response to disrupted traffic on inclines, facilitating traffic flow and stemming losses of foragers and prey. Informed by our observations, we present a theoretical model based on proportional control and negative feedback, which may be relevant to many distributed systems in which group-level properties can be modified through individual error sensing and correction. The mechanism is simple, and ants only require information about their individual state.

Author contributions: M.J.L., C.R.R., S.G., and I.D.C. designed research; M.J.L. performed research; M.J.L., C.R.R., C.J.L., A.B.K., and S.G. analyzed data; and M.J.L., C.R.R., C.J.L., A.B.K., S.G., and I.D.C. wrote the paper.

The authors declare no competing interest.

This article is a PNAS Direct Submission.

[1]M.J.L. and C.R.R. contributed equally to this work.

[2]To whom correspondence may be addressed. Email: matthew.lutz@gmail.com or chrisreidresearch@gmail.com.

This article contains supporting information online at https://www.pnas.org/lookup/suppl/doi:10.1073/pnas.2013741118/-/DCSupplemental.

Published April 23, 2021.

Unlike most ants that maintain a fixed nest location, colonies alternate every few weeks between a stationary and a nomadic phase, during which the entire colony moves nightly to a new temporary nest site, known as a bivouac (22, 23). Most workers spend the day foraging in massive swarm raids that start at dawn, combing the forest floor to flush out a diverse array of arthropod prey from the leaf litter (24, 25). At the front of the raid, fleeing prey items are attacked en masse, with those caught dismantled for transport along a branching trail network that can stretch for over 100 m back to the bivouac (26). Raids must be conducted at a rapid pace to maintain the high rates of prey delivery needed to support the ravenous appetite of the developing brood (27). This evolutionary pressure has led to a number of morphological and behavioral adaptations, including the spontaneous formation of traffic lanes that increase the efficiency of foraging trails (10), some of the highest running speeds among all ants (28), and a specialized porter caste morphology to facilitate the transport of bulky prey items, carried under the body (29).

This suite of adaptations includes the remarkable capacity for self-assembly, by which ants can join together to create temporary structures that modify the environment (27, 30, 31). Various examples of self-assembly have been observed in other social insects (32, 33), and these structures have been described as intermediate-level parts of insect societies—adaptive units that function at a level between individual and colony (34). For *E. burchellii* and the closely related *Eciton hamatum*, self-assembled structures serve two primary functions: for shelter, in the case of the bivouac, and to facilitate the flow of traffic during raids and emigrations, with structures like plugs (27) and bridges (30, 31) that emerge along the trail network as needed. Our previous work on *Eciton* bridges has shown how these structures are robust to perturbations and responsive to traffic and environmental geometry, changing size and location to create shortcuts that benefit the colony.

Here we reveal another type of self-assemblage in *E. burchellii* which we call "scaffolds," given their function as temporary support structures. These structures have not been previously studied experimentally or clearly defined, although they have been described based on observations in previous literature without consistent terminology (35, 36). Scaffolds often form when the foraging trail crosses a sloped surface from which ants may slip and/or fall, such as a rock face, tree root, or even the wall of a building (as shown in *SI Appendix*, Movie S1). To form a scaffold, individual ants stop and grip the underlying surface with their tarsi, remaining stationary as traffic continues to pass. Scaffolds can be sparse, consisting of only a few dispersed ants, or extremely dense, with many ants overlapping one another in a continuous cluster (Fig. 1 and *SI Appendix*, Movie S2). To ascertain how scaffolds form and under what conditions, and to assess their effects on foraging traffic, we conducted field experiments with wild colonies of *E. burchellii*, using an apparatus that allowed for manipulation of the slope over which ants traversed (Fig. 1). We observed and quantified the growth of scaffold structures and measured traffic variables to assess their influence on scaffold formation.

Our experimental results show that scaffolds repeatedly and predictably form on inclined surfaces, and we describe the relative influences of environmental and traffic variables on their growth. Informed by these observations, we propose a theoretical model that describes scaffold growth as a control response at the group level that emerges through a simple process of error correction at the individual level. Our model describes a hypothetical mechanism underlying scaffold formation that links individual-level sensing of disruption to the adaptive collective response of scaffold formation. Comparing the model predictions with our experimental observations, we show that the model captures well the observed dynamics of scaffold growth, and we derive an analytical solution that allows for straightforward prediction of these dynamics.

Results

Field experiments were conducted on Barro Colorado Island, Panama, in January and February 2015. The experimental apparatus consisted of two platforms three-dimensionally (3D) printed from PLA filament, each mounted on a flexible tripod 10 to 15 cm above the ground, linked together with an adjustable hinged panel (Fig. 1). The slope of this panel could be fixed at 10° increments, from nearly horizontal (20°) to vertical (90°), using a series of removable spacers, and it was covered with sandpaper

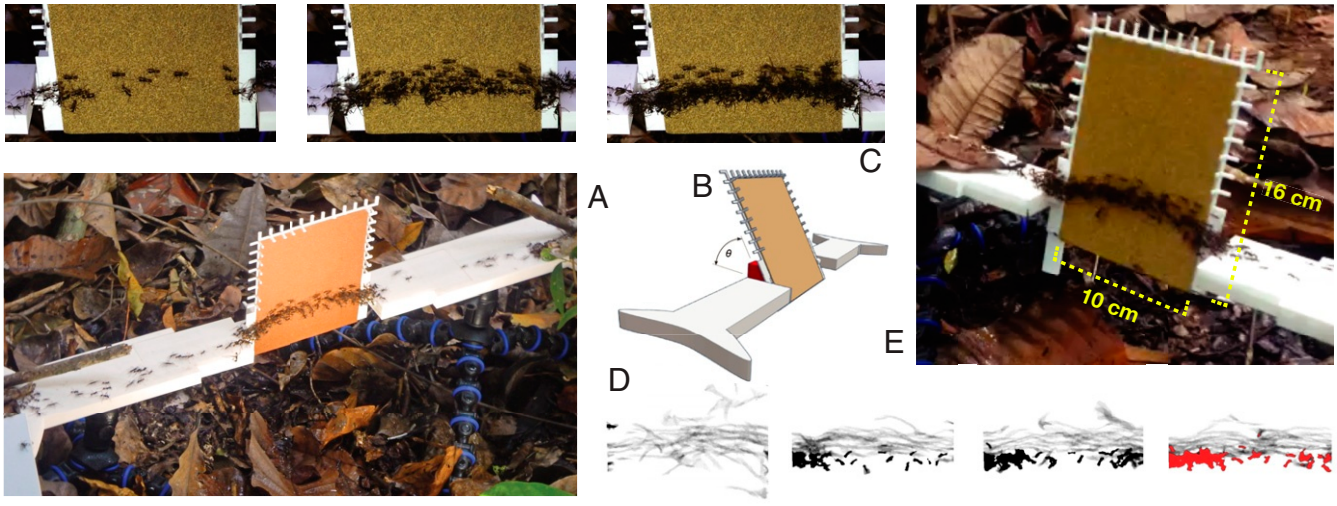

Fig. 1. Overview of experimental apparatus and video analysis procedure. (*A*) Photo of apparatus setup in the field during an experiment, with platform set to 90°. (*B*) Diagram of 3D-printed apparatus assembly, with removable spacer to adjust platform angle shown in red. (*C*) Frames extracted from video of experiment with platform set to 90°, at experiment start (*Left*), after 120 s (*Middle*), and after 300 s (*Right*). (*D*) Diagram of image subtraction algorithm for video analysis. Moving ants are shown in gray, with stationary ants shown in black (indicating scaffold area over time) and the final scaffold area shown in red. (*E*) Dimensions of adjustable platform overlaid on photo of experiment in progress, with platform set to 80° (removable spacer to adjust angle visible at bottom left of platform).

to provide a naturalistic surface that ants could grip (as tested in pilot experiments). Before each experiment, foraging traffic was interrupted as the apparatus was cleared of ants and set to one of the treatment angles. When ants reestablished traffic across the platform, video recording commenced (marking the start of an experiment) and continued for 10 min (until experiment end). The angle of the sloped platform was the only factor directly manipulated since the rates of traffic and prey delivery fluctuate throughout the course of a raid. In total, 89 experiments were conducted, with either 10, 11, or 12 trials completed at each of the eight angle treatments, from 20° to 90°. After processing the videos, 4 trials had to be removed due to issues with recording quality, leaving a total of 85 trials for the main analyses, which involved estimating the rates of traffic and prey delivery and final scaffold size. For higher-resolution analyses involving estimates of scaffold growth over time (Fig. 2*A* and *Model Fitting, Parameter Estimation, and Validation*), an additional 15 trials had to be removed due to variations in lighting (see *Materials and Methods* for details).

Dynamics of Scaffold Growth. Scaffolds formed more often and grew larger on steeper slopes (Fig. 2*B*). We defined a stable scaffold as consisting of five or more ants stopped on the platform after 10 min. Scaffolds rarely formed on slopes of less than 40° (4.76% of experiments, $N = 1$ of 21), and they were far more likely to form at or above this threshold (81.25% of experiments, $N = 52$ of 64; see *SI Appendix*, Table S1, for summary data from each angle).

To examine the effects of the experimental variables on scaffold size, we fitted a linear mixed-effects model, using a negative-binomial distribution with linear parameterization, with the Generalized Linear Mixed Models using Template Model Builder (glmmTMB) package for R [version 1.0.1 (37, 38)]. The mean traffic flow rate (ants per second), prey delivery rate (prey-carrying ants per second), and log-transformed surface angle θ (degrees) were examined as fixed effects, with experiment date treated as a random effect to control for between-colony variations (the proportion of bidirectional traffic was considered as another possible fixed effect but correlated strongly with overall traffic so was not included). Models containing all possible combinations of the fixed effects and their interactions were ranked using the Bayesian information criterion (BIC), and the model with the lowest BIC was selected for this analysis. The final model contained the fixed effects of surface angle θ and prey delivery rate, along with the random effects of experiment date. Residual diagnostics (*SI Appendix*, Fig. S1) were obtained using the simulation-based approach implemented in the Diagnostics for HierArchical Regression Models (DHARMa) package for R [version 0.3.0 (39)]. As shown in Fig. 2*C*, our mixed-effects model showed that the angle of the surface, θ (log-transformed), was the strongest predictor of final scaffold size (standardized effect size $=13.63$; $p < 0.001$), followed by prey delivery rate (standardized effect size $=1.39$; $p < 0.001$). Model predictions of final scaffold size at different angles and rates of prey delivery are shown in *SI Appendix*, Fig. S3.

Effects of Scaffolds on Foraging Traffic. To assess how scaffold formation affected the flow of traffic, we counted the number of ants slipping and/or falling when crossing the experimental platform for 2 min at the beginning and end of each experiment. Fig. 3 shows the proportion of ants that slipped and/or fell entirely from the apparatus during these time windows, at each angle. To examine the effect of the environmental geometry on the proportion of ants slipping and/or falling, we fitted a linear mixed-effects model using a binomial distribution [glmmTMB package for R, version 1.0.1 (37)]. Surface angle θ (degrees) and time (either beginning or end of experiment) were used as fixed effects, with the date of experiment again treated as a random effect to control for between-colony variations. Models containing all possible combinations of the fixed effects and their interactions were ranked using the BIC, and the model with the lowest BIC was selected for this analysis. The final model contained the two aforementioned fixed effects, plus their interaction. Model diagnostics were performed by visually inspecting the random effect quantiles (shown in *SI Appendix*, Fig. S4).

This model showed that the surface angle θ was a significant predictor of the proportion of ants slipping and/or falling (standardized effect size $=0.71$; $p < 0.001$; see *SI Appendix*, Fig. S5).

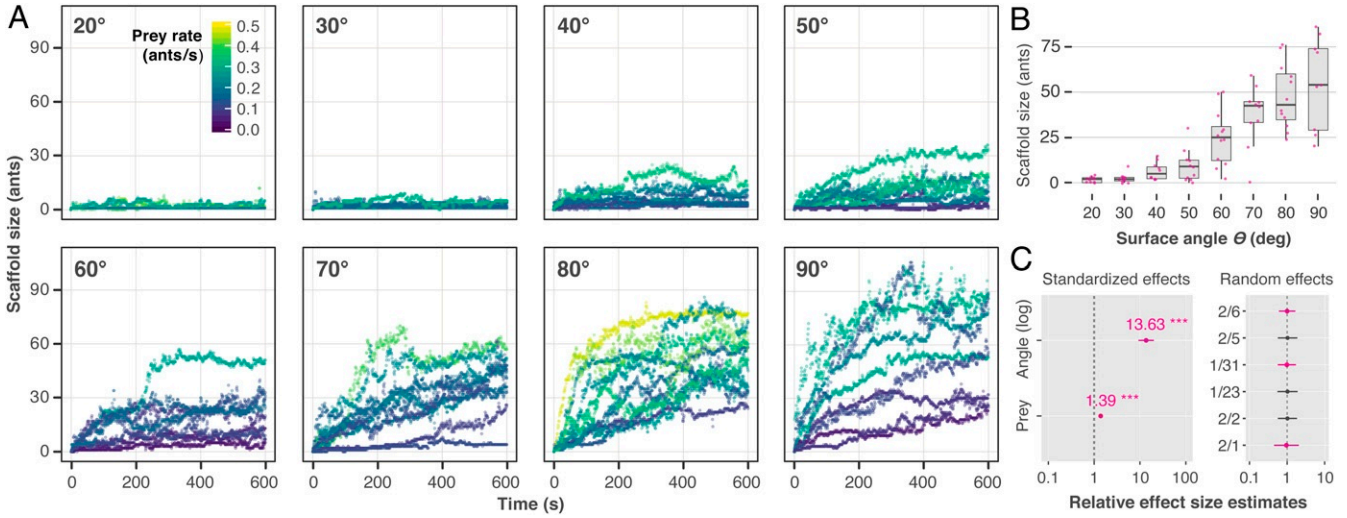

Fig. 2. Scaffold growth data and results from mixed-effects model. (*A*) Growth curves showing scaffold size over time, grouped by angle treatment. Points indicate scaffold size at each second, measured by the software in pixel area, then converted to estimates of the number of ants in a structure, by scaling based on manual ground-truth counts. Color scale indicates rate of prey transport for each experiment. Total $N = 70$, with N for each angle from 20° to 90° = 5, 7, 9, 10, 9, 10, 11, and 9. (*B*) Box plot showing summary data of final scaffold size, grouped by angle. Pink dots indicate final values for each experiment. Total $N = 85$, with N for each angle from 20° to 90° = 10, 11, 10, 11, 12, 10, 12, and 9. (*C*) Results from the linear mixed-effects model, showing the standardized relative effects of each of the predictors on final scaffold size (expressed as incidence rate ratios). (*Left*) Relative strengths of fixed effects and (*Right*) relative strengths of random effects (date of experiment).

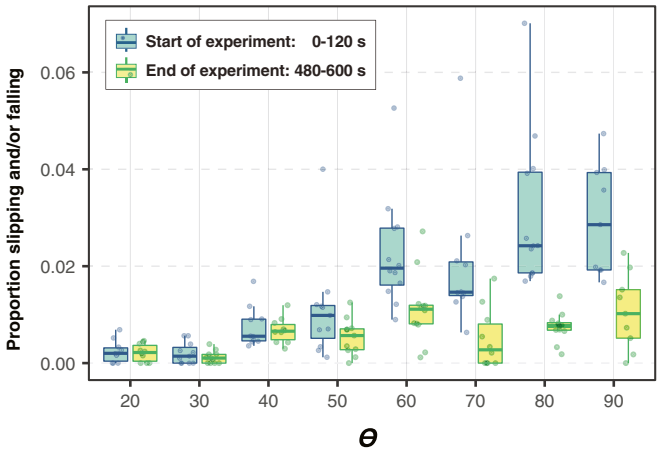

Fig. 3. Effects of scaffold formation on traffic disruption. Comparison between the proportion of ants slipping and/or falling while crossing the experimental platform during the first and last 2 min of each experiment (representing the absence or presence of scaffold structures, respectively).

It also revealed a significant interaction between θ and experimental time (standardized effect size $= -0.39$; $p < 0.001$), indicating that the proportion of ants slipping and/or falling increased with θ at the beginning of an experiment but did not change along with θ when measured at experiment end (*SI Appendix*, Fig. S6). Thus, our model revealed that the proportion of ants slipping and/or falling was no longer affected by the slope of the surface after scaffolds formed, explaining the differences observed in Fig. 3.

Theoretical Model of Scaffold Growth. Informed by these experimental results, we developed a theoretical model to explore the potential mechanism underlying scaffold growth that links individual sensing of environmental properties with the group-level adaptive response of scaffold formation. The model is inspired by the concept of proportional control, whereby a system-wide control response is applied in proportion to some error signal at a given time. A simple example of such a negative feedback loop can be found in an automobile's cruise control system, in which the amount of throttle applied at any time is proportional to the difference between the current and desired speeds. Hence, low speeds will induce a stronger throttle response, which tapers off as speed increases and error decreases.

Here we consider the systemic error to be traffic disruption due to ants slipping and/or falling along an inclined surface, while the formation of a scaffold that alleviates this disruption can be seen as a system-level control response. As scaffolds grow over time, fewer ants slip (as shown in Fig. 3), and the systemic disruption is gradually reduced until the structure reaches a stable size. The error is detected at the individual level, resulting in a distributed proportional control response.

The model consists of a pair of coupled differential equations describing the relationship between scaffold growth and the overall slipperiness of the surface over time. These are denoted by two state variables A and S, where $A(t)$ is the scaffold size at a given time (in number of ants) and $S(t)$ characterizes the physical properties of the surface, with respect to how likely ants are to slip when traversing. Based on our observations, we hypothesize that ants have a tendency to stop and join scaffolds that can be triggered by temporarily losing their footing (or slipping), then regripping the surface. This is formalized in the model as the parameter $P_{J|S}$, which describes the conditional probability of an ant that has slipped to join a scaffold.

The mean overall probability of slipping while crossing a surface (including ants that join scaffolds and those that do not) is denoted P_S. Since this term captures the effects of the environment on ant traffic, it can be used as a proxy estimate for the slipperiness of the surface ants traverse. This is denoted by the other state variable S, a measure of how likely a particular geometry is to cause slipping (and thus increased traffic disruption). We distinguish the surface property S from the ant property P_S, although they map to one another, such that crossing a surface with slipperiness S correlates with a probability of slipping P_S for individual ants.

From P_S and $P_{J|S}$, we can find the overall probability of an ant joining a scaffold using the multiplication rule of probability (as described in *Materials and Methods*). Given the correspondence described above, we substitute S for P_S into this calculation and introduce a flow rate of ants, μ, to derive the first model equation. This describes the change in scaffold size A over time as

$$\frac{dA}{dt} = \mu P_{J|S} S, \qquad [1]$$

where μ describes the rate of ants that can potentially join a scaffold when crossing a surface. The rate μ is estimated from the observations for each trial by subtracting the rate of prey delivery from the overall traffic rate since ants carrying prey do not join scaffolds. While traffic can fluctuate over the time scale of an experiment (as shown in *SI Appendix*, Fig. S6), the model assumes a constant flow rate as an input for tractability. We also examined a model that included ants leaving the scaffold, but since this behavior is relatively infrequent compared to ants joining the scaffold, at least on the time scale of our experiment, the results were comparable and, in many cases, inferior to the model described here (see *SI Appendix*, *Materials and Methods*, for details).

Informed by our results that show slipping to be reduced over time by scaffold formation (Fig. 3), we propose a second differential equation to describe this reduction in slipperiness as a function of scaffold growth, where S is reduced (with respect to its current value) in proportion to scaffold size A at time t, at a rate described by

$$\frac{dS}{dt} = -\beta\theta p S A, \qquad [2]$$

where p is the proportion of traffic made up of prey-carrying ants and θ is the angle of the slope, in radians. The coefficient β is a scaling factor, which can be fixed as a constant across all experiments, as described in the following section. This allows the model to be fitted to the data from each trial to generate estimates for the two unknown parameters $P_{J|S}$ from Eq. **1**, a property of individual ants, and the initial value of S, a property of the environment. We solve this system of ordinary differential equations (ODEs) numerically and perform model fitting using an optimization routine to generate these parameter estimates as follows.

Model Fitting, Parameter Estimation, and Validation. The ODE system above was solved numerically for A and S over a time span of 600 s, corresponding to the duration of an experiment, using the ode45 solver in MATLAB (R2020b). With the observations of scaffold size over time for each trial, optimization was performed using a nonlinear least-squares approach to generate fitted estimates for $P_{J|S}$ and the initial value of S_0, with the lsqcurvefit function and MultiStart solver (to avoid local minima). Corresponding experimental variables for each trial were input from our observations, including μ and p, measured from the rates of traffic and prey delivery, and surface angle θ. We interpret the coefficient β as a scaling factor that can be fixed as a constant, to focus on the effects of the two fitted parameters of biological interest. To test this, we first treated β as another free parameter to be fitted. As shown in *SI Appendix*, Fig. S7, estimates of

its value varied widely but only at the lowest angles, representing cases where only small scaffolds formed. Thus, we considered β to have been overfitted in these cases to compensate for measurement noise with small or unstable scaffolds. To avoid such overfitting, we determined that the model could still perform well if β was fixed across all experiments instead, and we fixed it at a constant value derived from the median of these estimates (for the results described here, $\beta = 0.0023$). This also allows for clear interpretation of the model results since both of the fitted parameters are biologically meaningful terms.

Since the model describes scaffold growth over time, the fitting procedure is only relevant for cases where scaffolds reached a stable size, and their growth over time could be estimated. Therefore, we fit the model to data from our experiments at and above 50°, where lighting and video quality were consistent enough for reliable growth estimates to be obtained ($N = 44$). For an initial approximation of the overall goodness of fit, we estimated R^2 values for each of these fits, resulting in a mean overall $R^2 = 0.48$ (SD $= 0.75$). Filtering out cases with extremely low estimates ($R^2 < 0.10$) revealed better fits among the remaining subset of 37 experiments (mean $R^2 = 0.70$; SD $= 0.17$). To complement these approximations, we examined the model fits in more detail by visual estimation. We plotted predicted growth curves along with their 95% prediction intervals over the experimental observations, using a bootstrapping procedure to generate distributions of the estimated parameters $P_{J|S}$ and S_0 to identify confidence intervals for the estimates. In addition, we generated another set of prediction intervals to capture the variation in traffic over the course of each experiment. Fig. 4*A* shows representative example fits at four different angles, with the results from all other experiments where the model was fitted ($N = 44$) shown in *SI Appendix*, Figs. S8–S12.

To validate the model, we compared its predictions of the slipperiness of the surface S with estimates from our observations of the quantity P_S, over the first and last 2 min of each experiment. As described above, P_S represents the total proportion of ants slipping over a given time, including those that join a scaffold (measured by the scaffold size at t) and those that do not (for which we used our counts of ants slipping, as described in *Effects of Scaffolds on Foraging Traffic*). If the surface property S can be expressed as a proxy measure of slipperiness in the same terms as P_S, and if the model captures how this property relates to the experimental variables, the predicted values of S output by the model should be close to our observed estimates of P_S, even though none of the slipping observations were used in the model fitting.

To summarize the model predictions over the first 120 s, we took the mean values of estimates for S at $t = 0, 60$, and 120, for each model run. As shown in Fig. 4*B*, the model predictions were similar to our experimental observations for P_S over the same time window, grouped by surface angle θ, predicting initially higher levels of slipperiness at steeper angles. Using the same procedure, we also estimated the mean values of S over the final 120 s of each experiment, using the estimates of S at t = 480, 540, and 600 s, to compare with the experimental measurements of the total slip probability P_S over this same time. As shown in Fig. 4*B*, our model also predicted well the reduction in surface slipperiness that we observed in our analysis of ants slipping while crossing the experimental surface and how this varied depending on the angle θ. Thus, the model predicted well the initial slip potential of the surface S_0 for each angle θ and how S was reduced over time by scaffold growth.

Analytical Solution. In addition to the numerical procedure above, the system of differential Eqs. **1** and **2** that constitute the model can be solved analytically, with the solution given by

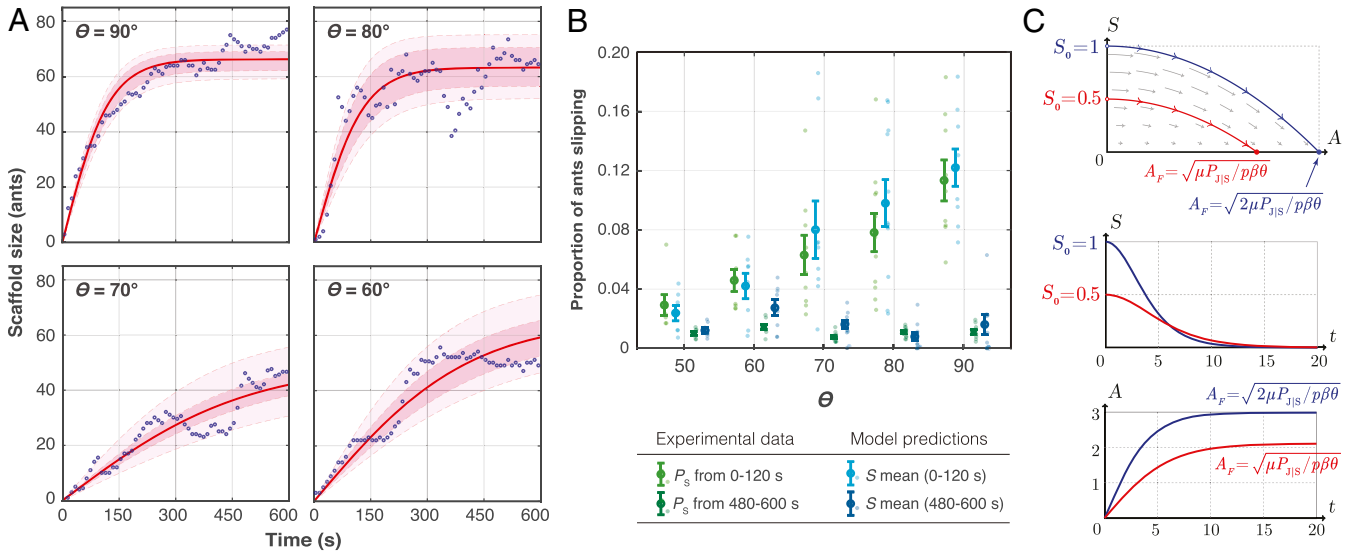

Fig. 4. Model predictions and analytical solution. (*A*) Examples of growth curves predicted by the model (red lines), with the corresponding experimental observations (blue circles), for one representative trial at each of four angles ($\theta = 60$, 70, 80, 90, as noted). Results from all experiments for which the model was fitted ($N = 44$) are shown in Figs. S8–S12, grouped by surface angle θ. Dark pink bands indicate 95% prediction intervals with the fitted estimates for S_0 and $P_{J|S}$, assuming constant traffic flow at the mean rate for each replicate. Light pink bands show 95% prediction intervals over the entire range of traffic, with lower bounds indicating predictions using the lowest rate as an input, and upper bounds using the highest. (*B*) Model predictions of *S* compared with experimental observations of P_S, the proportion of ants slipping (estimated as described in *Materials and Methods*). Mean predicted values of *S* over 0 to 120 s are shown as light blue open circles, with estimates of P_S over the same time shown in light green. Corresponding values from 480 to 600 s are shown in dark blue and dark green, respectively. Large circles and error bars indicate means and SEM, respectively (total $N = 44$, N from 50° to 90° = 7, 8, 9, 11, and 9). (*C*) (*Top*) Phase portrait of analytical solution dynamics, obtained using Eq. **6**, with two sample system trajectories. Since probability values cannot exceed 1, the phase portrait is restricted to the region beneath the blue trajectory. Start and end states of trajectories are indicated with empty and filled circles, respectively, with gray arrows denoting vector field of the solutions. (*Center* and *Bottom*) Model solutions corresponding to these system trajectories, with $\mu = 1$ and $\beta = 1$, showing slipperiness, *S*, and scaffold size, *A*, over time.

$$A = \sqrt{\frac{2\,\mu S_0 P_{\mathrm{J|S}}}{p\beta\theta}}\,\tanh\left(t\sqrt{\frac{\mu p\beta\theta S_0 P_{\mathrm{J|S}}}{2}}\right), \qquad [3]$$

$$S = S_0 - S_0\tanh\left(t\sqrt{\frac{\mu p\beta\theta S_0 P_{\mathrm{J|S}}}{2}}\right)^2. \qquad [4]$$

The parameters are as described above, with the initial conditions $A(0)=0$ and $S(0)=S_0$. This solution can be used to generate straightforward predictions of some aspects of the system behavior and model output given certain experimental observations or estimates. For instance, the overall size of a scaffold tends to a final value A_F, which is given by

$$A_F = \sqrt{\frac{2\,\mu S_0 P_{\mathrm{J|S}}}{p\beta\theta}}. \qquad [5]$$

The model predicts that scaffolds grow most rapidly at the start, before slowing down and settling at A_F, and the probability of ants slipping (and potentially joining) decreases as they grow, tending to zero as scaffolds approach their maximum size. This is consistent with the following phase portrait analysis of the system, which demonstrates that such behavior must necessarily arise in any solution of the model. First, we combine both parts of [**1**] and [**2**], which gives

$$\frac{dS}{dA} = -\frac{p\beta\theta A}{\mu P_{\mathrm{J|S}}}, \qquad [6]$$

to produce a phase portrait describing the relationship between $A(t)$ and $S(t)$ as the system evolves (Fig. 4*C*). Each trajectory of the system begins at some $(A,S)=(0,S_0)$, and as the system evolves, scaffold size increases, and the probability of slipping, and thus joining, decreases. The trajectory tends to some value $(A,S)=(A_F,0)$, where the probability of slipping is 0, and the size is therefore fixed at some A_F. This analysis makes clear that adjusting the value of S_0, maintaining all other model parameters, has the effect of reducing the final scaffold size.

Discussion

Our experimental results reveal that *E. burchellii* army ants consistently form scaffold structures when crossing surfaces inclined beyond a threshold of around 40°, above which ants begin to lose their footing. Scaffolds are responsive to local environmental geometry and specific traffic conditions: steeper slopes and higher rates of prey delivery and traffic are all associated with the formation of larger structures. When they form, scaffolds exhibit a saturating growth response, growing rapidly at first, then settling to a final size, which is a predictable function of the environmental variables. We also identify some of the functional benefits that scaffolds provide for the colony, including reducing losses of foragers and prey and alleviating traffic disruption.

Informed by these results, our theoretical model offers a simple and plausible mechanistic explanation of scaffold formation. It describes scaffold growth as a response at the collective level, akin to a form of distributed control, which results from a process of individual error correction. As observed in our experiments, ants crossing steeper inclines are more likely to slip, and we hypothesize that ants stop to join scaffolds with a conditional probability that depends on slipping, responding to this stimulus by attaching to the surface and remaining stationary. Our experimental observations quantify how scaffold formation reduces the probability of slipping over time, and the model predicts the initial slipperiness of a surface at a given slope and how this is reduced over time as scaffolds grow. These predictions emerge from the model even though none of our experimental observations of ants slipping are used as inputs for the model or for the model-fitting procedure. The model captures the growth dynamics of scaffolds across a range of traffic conditions, providing insight into how particular combinations of traffic and environmental geometry influence their growth.

The growth rate and ultimate size of scaffolds are emergent properties that can arise from individual sensing and error correction, without the need for complex communication, enabling a system-level response that is suited to each particular configuration of traffic and environmental geometry. The error in this system is detected at the individual level, and individual error correction leads to the emergent group-level response of scaffold growth. This individually sensed error may be ants responding to their own slipping, experiencing disruption due to other ants slipping at an increased rate, or some combination of such stimuli. In any case, this error is reduced by the formation of scaffolds and is detected at the individual level; therefore, we consider this a distributed form of proportional control.

In an early description of army ant self-assembly from 1874 (40), the naturalist Thomas Belt asked, "Can it not be contended that such insects are able to determine by reasoning powers which is the best way of doing a thing, and that their actions are guided by thought and reflection?" Indeed, many dramatic examples of collective animal behavior were long thought to result from sophisticated reasoning capabilities or even unknown mechanisms involving thought transfer. However, research on collective behavior has revealed common principles that explain complex group-level behaviors as the result of relatively simple individual rules and local interactions (41, 42). A key challenge in understanding these principles is ascertaining how inputs from individual-level sensors are combined and filtered to produce group-level outputs (43), and such insights have come to inform the design of complex engineered systems that rely on distributed forms of control (44). Thus, while the experiments described here involved ants crossing an inclined surface, our results may be relevant to other systems in which group-level properties can be modified via individual error sensing and correction.

As human technological and social systems increase in complexity, the need for simple, robust mechanisms for error correction to rapidly respond to systemic disruption at multiple scales without relying on complex communication or oversight is paramount. Such simple mechanisms can avoid some of the pitfalls that often arise from communication within groups like biases (45, 46) that result from the oversharing of correlated information (47, 48), and the model presented here may inform approaches to addressing these. Our model and experimental results should provide insights for the field of swarm robotics as well (49–51), in which increasingly complex group behaviors, including self-assembly (52), are often constrained by technical limitations on both individual sensors and communication capabilities (53).

In this context, our model relates to previous models of self-organized aggregation that have informed the development of robotic systems, such as models of cockroach aggregation in which individuals assess others already in a cluster (50, 54–56) or corpse piling in ants, where individuals respond to corpses already deposited, and to other ants (57, 58). However, the mechanism we have identified requires less complex sensing since the ants need only to respond to their own slipping and do not need to assess the size of a structure in place. This describes scaffold growth as a rapid, on-demand response that alleviates disruption that would otherwise result from the dynamic environmental conditions. With minimal requirements for sensing and information processing, this finding may also be relevant at smaller scales, for the design of self-healing materials (59–61) and future developments in biofabrication (62, 63).

Materials and Methods

Experimental Protocol, Site, and Study Organism. Field experiments were conducted in the seasonal tropical forest of Barro Colorado Island, Panama, in daylight hours during the dry season in January and February 2015. Three different colonies of *E. burchellii foreli* (Mayr), all in the nomadic phase, were located and used in experiments for 2 or 3 d each. Experiments were performed along the primary raiding trail, where traffic is most consistent throughout the day, within 50 m of the bivouac (temporary nest site). Each morning a suitable location along this trail was found, with enough space to set up the experimental apparatus and recording equipment. A break was created in the existing trail by removing sticks and leaves from the substrate, and the apparatus was inserted into the resulting gap. A field compass with spirit level was used to adjust the side platforms to be level and in plane with one another when setting up the apparatus. The flow of ant traffic was redirected up onto both ends of the apparatus using the displaced sticks and leaves as makeshift ramps, which were covered in trail pheromone from preexisting traffic. An experiment was considered to begin once the first ant had reestablished a continuous flow of traffic over the apparatus, and each experiment was recorded for 10 min from this point.

Data Collection and Extraction. Videos were filmed with a high-definition camcorder (Panasonic HDC-300) at 30 fps. The camera was mounted on a tripod and positioned perpendicular to the surface being filmed, at a distance of approximately 60 cm. After initial processing of the video footage, 4 experiments were discarded due to issues with the experimental setup or recording, leaving a total of 85 experiments used for the analyses in *Dynamics of Scaffold Growth* and *Effects of Scaffolds on Foraging Traffic*. These involved measuring the traffic variables as described below and final size of scaffolds. Out of these, 70 experiments were used for further analyses of scaffold growth over time using the automated method described below, with 15 videos that could not be analyzed at higher temporal resolution due to wide variations in lighting (although we could still estimate the final scaffold size and traffic counts, so these could be used for the first part of the analysis).

The rate of ant traffic for each experiment was measured by visual counts taken of each video, slowed to 0.25× speed using VLC media player. The total number of ants crossing the edge of the experimental surface in each direction was counted during three 30-s windows over the course of each 10-min experiment—from 00:30 to 01:00, from 05:00 to 05:30, and from 09:00 to 09:30. Counts from both directions were combined, and these totals were divided by 30 s to give an estimate of the traffic rate at experiment start, middle, and end, in ants per second. The mean of these three rates was taken as an estimate of the overall traffic rate for each experiment. The proportion of bidirectional traffic was calculated by dividing the traffic flow in the nondominant direction by the overall traffic flow. The rate of prey delivery was estimated in a similar way, by manually counting the number of prey items transported for the duration of each experiment (at full speed). The total number of prey-carrying ants was divided by 600 (s), giving a value for the prey delivery rate in prey-carrying ants per second.

Visual counts were also made of the number of ants that slipped and/or fell from the platform when crossing. These counts were performed for the first 2 min and last 2 min of each experiment, to estimate the effects of the presence or absence of scaffold structures (in those cases where one formed). A slip was defined as a sudden vertical displacement of more than one body width, in which an ant crossed a line estimated as the lower boundary of the trail across the platform (or the structure, if one formed). A fall was counted if an ant fell completely from the platform.

The size of scaffolding structures over time was measured using a custom image subtraction algorithm in MATLAB R2016b (version 9.0). Subsequent frames of the videos were compared to detect and record whenever an ant remained stationary (joined a structure) rather than moving with the flow of traffic (Fig. 1*D*). Output from the software was given in pixel area, then these estimates were rescaled by comparison with manual ground-truth counts to estimate the number of ants within a scaffold (see *SI Appendix, Materials and Methods*, for details of the scaling procedure).

Probability Estimates for Theoretical Model. To derive the probability estimates underlying the theoretical model, we first make the simplifying assumption that all ants joining a scaffold have slipped. This does not require an explicit definition of what constitutes a slip, so we can state more generally that all scaffold ants have experienced some slipping-related stimulus. Since scaffolds do not form on level surfaces and only rarely form on shallow slopes, as our data show, we consider this a reasonable assumption.

This assumption can be expressed as the conditional probability $P(slip|join)$, or the probability that an ant has slipped (or experienced some slipping-related effect, e.g., from traffic disruption or collisions) given it has joined a scaffold. Assuming this is the case for all joining ants, the conditional probability $P(slip|join)$ will be equal to 1. From this value, we can estimate the inverse conditional probability $P(join|slip)$, or the probability that an ant will join a scaffold, given it has slipped. Based on our observations, we hypothesize that this individual-level response may be crucial to the mechanism of scaffold growth, so we use Bayes's theorem $P(A|B) = P(B|A)P(A)/P(B)$ to estimate it as follows:

$$P(join|slip) = \frac{P(slip|join)\,P(join)}{P(slip)}. \quad [7]$$

Since the other conditional probability, $P(slip|join)$, is assumed to be equal to 1, we can simplify and rearrange the above equation in terms of a quantity we can relate directly to our experimental data, the term $P(join)$, which describes the overall probability of an ant to join a scaffold:

$$P(join) = P(join|slip)\,P(slip). \quad [8]$$

From this relationship, we derive Eq. **1** of our model of scaffold growth directly, in its simplest form, by incorporating a traffic flow rate of ants, a proportion of which are induced to join a scaffold when crossing the surface, given by $P(join)$. This results in a rate of ants joining over time, corresponding to the change in scaffold size, dA, in our model. We rename the conditional probability $P(join|slip)$ to $P_{J|S}$ for simplicity and reformulate the term $P(slip)$ as a measure of the effect of environmental geometry on ant traffic (S, or slipperiness), rather than an internal ant property. However, the two can still be compared in the same terms (as a proportion of ants slipping), and we retain the term $P(slip)$ (shortened to P_S) when referring to a property of ants.

P_S describes the overall probability of an ant slipping at a given time. Therefore, this accounts for ants that join scaffolds (assumed to have slipped) as well as those that slip and continue walking, both of which can be estimated from our experimental observations. To compare the observed estimates of P_S to the predicted values of S from the model, this value is calculated using the following, as derived from a conditional probability table:

$$P_S = \frac{N_{\text{ants slip, join}} + N_{\text{ants slip, do not join}}}{N_{\text{total ants crossing}}}. \quad [9]$$

We consider the fact that estimates of P_S from our data, obtained by this method, correspond quite well with model estimates of the mean values of S over the same time windows (output from numerically solving the model's differential equations) to offer strong support for the model's validity.

Data Availability. All study data are included in the article and *SI Appendix*. All code used in the study for data analysis are available at GitHub, https://github.com/matthewlutz/army_ant_scaffolds.

ACKNOWLEDGMENTS. M.J.L. and C.R.R. thank the staff of the Smithsonian Tropical Research Institute and residents of Barro Colorado Island and James Herndon for the photograph of the apparatus in Fig. 1*A*. This work was supported by the NSF (IOS-1355061), the Office of Naval Research (N00014-19-1-2556), the Deutsche Forschungsgemeinschaft (German Research Foundation) under Germany's Excellence Strategy–EXC 2117-422037984, and the Max Planck Society (to I.D.C.); Australian Research Council Discovery Project 190101190 (to C.J.L.); Australian Research Council Discovery Early Career Researcher Award DE190101513 (to C.R.R.); and Princeton University's Department of Ecology and Evolutionary Biology (to M.J.L.). A.B.K. was supported by a Baird Scholarship and Omidyar Fellowship from the Santa Fe Institute.

1. E. J. T. Middleton, T. Latty, Resilience in social insect infrastructure systems. *J. R. Soc. Interface* **13**, 20151022 (2016).
2. B. Walker, C. S. Holling, S. Carpenter, A. Kinzig, Resilience, adaptability and transformability in social-ecological systems. *Ecol. Soc.* **9**, 5 (2004).
3. M. Burd, Ecological consequences of traffic organisation in ant societies. *Physica A Stat. Mech. Appl.* **372**, 124–131 (2006).
4. T. Bochynek, B. Meyer, M. Burd, Energetics of trail clearing in the leaf-cutter ant atta. *Behav. Ecol. Sociobiol.* **71**, 14 (2016).
5. B. S. Kerner, Experimental features of self-organization in traffic flow. *Phys. Rev. Lett.* **81**, 3797–3800 (1998).
6. D. Chowdhury, L. Santen, A. Schadschneider, Statistical physics of vehicular traffic and some related systems. *Phys. Rep.* **329**, 199–329 (2000).

7. D. Helbing, Traffic and related self-driven many-particle systems. *Rev. Mod. Phys.* **73**, 1067 (2001).
8. R. Louf, M. Barthelemy, How congestion shapes cities: From mobility patterns to scaling. *Sci. Rep.* **4**, 5561 (2014).
9. A. Dussutour, V. Fourcassié, D. Helbing, J. L. Deneubourg, Optimal traffic organization in ants under crowded conditions. *Nature* **428** (6978), 70–73 (2004).
10. I. Couzin, N. Franks, Self-organized lane formation and optimized traffic flow in army ants. *Proc. R. Soc. London Ser. B Biol. Sci.* **270**, 139–146 (2003).
11. E. Fonio *et al.*, A locally-blazed ant trail achieves efficient collective navigation despite limited information. *eLife* **5**, e20185 (2016).
12. T. Schmickl, I. Karsai, Integral feedback control is at the core of task allocation and resilience of insect societies. *Proc. Natl. Acad. Sci. U.S.A.* **115**, 13180–13185 (2018).
13. J. M. Pasteels, J. L. Deneubourg, S. Goss, Self-organization mechanisms in ant societies. I: Trail recruitment to newly discovered food sources. *Experientia Suppl.* **54**, 155–175 (1987).
14. R. Beckers, J. L. Deneubourg, S. Goss, J. M. Pasteels, Collective decision making through food recruitment. *Insectes Soc.* **37**, 258–267 (1990).
15. E. Bonabeau, G. Theraulaz, J. L. Deneubourg, Group and mass recruitment in ant colonies: The influence of contact rates. *J. Theor. Biol.* **195**, 157–166 (1998).
16. T. D. Seeley *et al.*, Stop signals provide cross inhibition in collective decision-making by honeybee swarms. *Science* **335**, 108–111 (2012).
17. C. Grüter *et al.*, Negative feedback enables fast and flexible collective decision-making in ants. *PLoS One* **7**, e44501 (2012).
18. T. J. Czaczkes, C. Grüter, F. L. W. Ratnieks, Negative feedback in ants: Crowding results in less trail pheromone deposition. *J. R. Soc. Interface* **10**, 20121009 (2013).
19. D. J. Kronauer, Recent advances in army ant biology (hymenoptera: Formicidae). *Myrmecol. News* **12**, 51–65 (2009).
20. S. O'Donnell, J. Lattke, S. Powell, M. Kaspari, Army ants in four forests: Geographic variation in raid rates and species composition. *J. Anim. Ecol.* **76**, 580–589 (2007).
21. J. L. Deneubourg, S. Goss, N. Franks, J. M. Pasteels, The blind leading the blind: Modeling chemically mediated army ant raid patterns. *J. Insect Behav.* **2**, 719–725 (1989).
22. N. R. Franks, C. R. Fletcher, Spatial patterns in army ant foraging and migration: Eciton burchelli on Barro Colorado Island, Panama. *Behav. Ecol. Sociobiol.* **12**, 261–270 (1983).
23. T. W. Soare, S. Tully, S. Willson, D. J. Kronauer, S. O'Donnell, Choice of nest site protects army ant colonies from environmental extremes in tropical montane forest. *Insectes Soc.* **58**, 299–308 (2011).
24. R. Chadab, C. W. Rettenmeyer, Mass recruitment by army ants. *Science* **188**, 1124–1125 (1975).
25. D. J. Kronauer, *Army Ants: Nature's Ultimate Social Hunters* (Harvard University Press, 2020).
26. T. Schneirla, Raiding and other outstanding phenomena in the behavior of army ants. *Proc. Natl. Acad. Sci. U.S.A.* **20**, 316–321 (1934).
27. S. Powell, N. R. Franks, How a few help all: Living pothole plugs speed prey delivery in the army ant Eciton burchellii. *Anim. Behav.* **73**, 1067–1076 (2007).
28. A. H. Hurlbert, F. Ballantyne, S. Powell, Shaking a leg and hot to trot: The effects of body size and temperature on running speed in ants. *Ecol. Entomol.* **33**, 144–154 (2008).
29. S. Powell, N. R. Franks, Ecology and the evolution of worker morphological diversity: A comparative analysis with Eciton army ants. *Funct. Ecol.***20**, 1105–1114 (2006).
30. S. Garnier *et al.*, Stability and responsiveness in a self-organized living architecture. *PLoS Comput. Biol.* **9**, e1002984 (2013).
31. C. R. Reid *et al.*, Army ants dynamically adjust living bridges in response to a cost-benefit trade-off. *Proc. Natl. Acad. Sci. U.S.A.* **112**, 15113–15118 (2015).
32. P. C. Foster, N. J. Mlot, A. Lin, D. L. Hu, Fire ants actively control spacing and orientation within self-assemblages. *J. Exp. Biol.* **217**, 2089–2100 (2014).
33. T. Bochynek, S. K. A. Robson, Physical and biological determinants of collective behavioural dynamics in complex systems: Pulling chain formation in the nest-weaving ant Oecophylla smaragdina. *PLoS One* **9**, e95112 (2014).
34. C. Anderson, G. Theraulaz, J. L. Deneubourg, Self-assemblages in insect societies. *Insectes Soc.* **49**, 99–110 (2002).
35. T. C. Schneirla, *Army Ants: A Study in Social Organization* (W. H. Freeman, 1971).
36. W. H. Gotwald, Jr, *Army Ants: The Biology of Social Predation* (Cornell University Press, 1995).
37. M. E. Brooks *et al.*, glmmTMB balances speed and flexibility among packages for zero-inflated generalized linear mixed modeling. *R J.* **9**, 378–400 (2017).
38. R Core Team, R: A Language and Environment for Statistical Computing (R Foundation for Statistical Computing, 2020). https://www.R-project.org/. Accessed 15 April 2021.
39. F. Hartig, DHARMa: Residual Diagnostics for Hierarchical (Multi-Level / Mixed) Regression Models. R package, Version 0.4.1. http://florianhartig.github.io/DHARMa/. Accessed 15 April 2021.
40. T. Belt, *The Naturalist in Nicaragua* (The Minerva Group, Inc., 2002), pp. 27–28.
41. A. Berdahl, C. J. Torney, C. C. Ioannou, J. J. Faria, I. D. Couzin, Emergent sensing of complex environments by mobile animal groups. *Science* **339**, 574–576 (2013).
42. I. D. Couzin, Collective cognition in animal groups. *Trends Cognit. Sci.* **13**, 36–43 (2009).
43. S. B. Rosenthal, C. R. Twomey, A. T. Hartnett, H. S. Wu, I. D. Couzin, Revealing the hidden networks of interaction in mobile animal groups allows prediction of complex behavioral contagion. *Proc. Natl. Acad. Sci. U.S.A.* **112**, 4690–4695 (2015).
44. N. Napp, R. Nagpal, Distributed amorphous ramp construction in unstructured environments. *Robotica* **32**, 279–290 (2014).
45. A. B. Kao *et al.*, Counteracting estimation bias and social influence to improve the wisdom of crowds. *J. R. Soc. Interface* **15**, 20180130 (2018).
46. B. Jayles, R. H. Kurvers, Debiasing the crowd: Selectively exchanging social information improves collective decision making. arXiv:2003.06863 (15 March 2020).
47. A. B. Kao, I. D. Couzin, Decision accuracy in complex environments is often maximized by small group sizes. *Proc. Biol. Sci.* **281**, 20133305 (2014).
48. J. Becker, D. Brackbill, D. Centola, Network dynamics of social influence in the wisdom of crowds. *Proc. Natl. Acad. Sci. U.S.A.* **114**, E5070–E5076 (2017).
49. J. Werfel, K. Petersen, R. Nagpal, Designing collective behavior in a termite-inspired robot construction team. *Science* **343**, 754–758 (2014).
50. N. Correll, A. Martinoli, Modeling and designing self-organized aggregation in a swarm of miniature robots. *Int. J. Robot Res.* **30**, 615–626 (2011).
51. F. Mondada *et al.*, SWARM-BOT: A new distributed robotic concept. *Auton. Robots* **17**, 193–221 (2004).
52. R. Groß, M. Bonani, F. Mondada, M. Dorigo, Autonomous self-assembly in swarm-bots. *IEEE Trans. Robot.* **22**, 1115–1130 (2006).
53. J. Werfel, D. Ingber, R. Nagpal, "Collective construction of environmentally-adaptive structures" in *2007 IEEE/RSJ International Conference on Intelligent Robots and Systems* (IEEE, 2007), pp. 2345–2352.
54. R. Jeanson *et al.*, Self-organized aggregation in cockroaches. *Anim. Behav.* **69**, 169–180 (2005).
55. S. Garnier, J. Gautrais, M. Asadpour, C. Jost, G. Theraulaz, Self-organized aggregation triggers collective decision making in a group of cockroach-like robots. *Adapt. Behav.* **17**, 109–133 (2009).
56. Y. Günzel *et al.*, Social modulation of individual preferences in cockroaches. *iScience* **24**, 101964 (2020).
57. G. Theraulaz *et al.*, Spatial patterns in ant colonies. *Proc. Natl. Acad. Sci. U.S.A.* **99**, 9645–9649 (2002).
58. C. Jost *et al.*, The interplay between a self-organized process and an environmental template: Corpse clustering under the influence of air currents in ants. *J. R. Soc. Interface* **4**, 107–116 (2007).
59. K. S. Toohey, N. R. Sottos, J. A. Lewis, J. S. Moore, S. R. White, Self-healing materials with microvascular networks. *Nat. Mater.* **6**, 581–585 (2007).
60. R. P. Wool, Self-healing materials: A review. *Soft Matter* **4**, 400–418 (2008).
61. M. D. Hager, P. Greil, C. Leyens, S. van der Zwaag, U. S. Schubert, Self-healing materials. *Adv. Mater.* **22**, 5424–5430 (2010).
62. P. Bajaj, R. M. Schweller, A. Khademhosseini, J. L. West, R. Bashir, 3d biofabrication strategies for tissue engineering and regenerative medicine. *Annu. Rev. Biomed. Eng.* **16**, 247–276 (2014).
63. R. F. Pereira, C. C. Barrias, P. L. Granja, P. J. Bartolo, Advanced biofabrication strategies for skin regeneration and repair. *Nanomedicine* **8**, 603–621 (2013).